NASA CONTRACTOR REPORT

NASA CR-1743

AERODYNAMIC BROADBAND NOISE MECHANISMS APPLICABLE TO AXIAL COMPRESSORS

by Robert A. Arnoldi

Prepared by
PRATT & WHITNEY AIRCRAFT
East Hartford, Conn. 06108
for

NATIONAL AERONAUTICS AND SPACE ADMINISTRATION • WASHINGTON, D. C. • MARCH 1971

1. Report No. NASA CR-1743	2. Government Accession No.	3. Recipient's Catalog No.
4. Title and Subtitle Aerodynamic Broadband Noise Mechanisms Applicable to Axial Compressors		5. Report Date March 1971 6. Performing Organization Code
7. Author(s) Robert A. Arnoldi		8. Performing Organization Report No. PWA-3930
9. Performing Organization Name and Address Pratt & Whitney Aircraft East Hartford, Conn. 06108		10. Work Unit No. 11. Contract or Grant No. NASW-1908
12. Sponsoring Agency Name and Address National Aeronautics & Space Administration Washington, D. C. 20546		13. Type of Report and Period Covered Contractor Report 14. Sponsoring Agency Code

15. Supplementary Notes

16. Abstract

A study of broadband noise produced by the interactions of turbulence (1) with the shock system upstream of a supersonic compressor and (2) with the surface of the rotor blade has been made. The dynamic response of the rotor blade in the latter interaction was constructed empirically, based on the results of a complementary experimental program. This program obtained the lift response of an instrumented airfoil subjected to periodic upwash fluctuations. Both source mechanisms are found to produce noise levels of significant magnitude; either might be a prime source of broadband engine noise, and further study of both is recommended.

The effect of incidence past stall on the unsteady response is shown to be a small reduction in magnitude and a slowly increasing delay in phase, neither of which make any substantial modifications in predicted noise output. This result was measured at a reduced frequency of 3.9; further investigations over a wider range is recommended.

17. Key Words (Selected by Author(s))	18. Distribution Statement
Aerodynamic Noise, Turbulence-Shock Interaction, Gust Loads, Unsteady Flow, Compressor Noise	Unclassified-Unlimited

19. Security Classif. (of this report)	20. Security Classif. (of this page)	21. No. of Pages	22. Price
Unclassified	Unclassified	48	$3.00

For sale by the National Technical Information Service, Springfield, Virginia 22151

PREFACE

This report describes the results of an investigation to evaluate certain broadband noise mechanisms applicable to axial compressors through analytical and experimental studies. This investigation was conducted by Pratt & Whitney Aircraft under the terms of National Aeronautics and Space Administration Headquarters Washington, D. C. Contract NASW-1908. The work was performed during the period 11 July 1969 through 30 June 1970.

The analytical study of broadband noise caused by interaction of turbulence with the shock system upstream of the rotor was conducted by Dr. John Blaisdell.

The experimental study of the heavily loaded airfoil response to a sinusoidal gust was conducted by G. Commerford under the supervision of F. Carta, both of the United Aircraft Research Laboratories. An examination of the implications of this experimental study to compressor broadband noise produced by turbulence-blade interaction was conducted by Dr. Robert A. Arnoldi.

TABLE OF CONTENTS

LIST OF ILLUSTRATIONS

LIST OF SYMBOLS

The following is a list of symbols used in this report.

BASIC SYMBOLS

a	- speed of sound in a stationary fluid
b	- semichord of airfoil
$\underline{c}$	- velocity of fluid relative to a stationary coordinate system
C_L	- lift coefficient of airfoil per unit span
c_p	- specific heat of fluid at constant pressure
dZ_i	- Fourier coefficient of the i^{th} disturbance (pressure, vorticity, etc.)
e	- energy density
$E(k_v)$	- energy-spectrum function
$\bar{f}^x_{m\mu}, \bar{f}^\theta_{m\mu}$	- modal series coefficient (axial, tangential) of spanwise distribution of fluctuating force amplitudes
$F(\phi'_p, \psi'_p, \eta)$	- a combination of transfer functions (equation 5)
$g(t)$	- random time dependence of the force per unit span on an airfoil, normalized through equation 17
$G(\omega)$	- power spectral function corresponding to g(t)
h	- hub-tip ratio
J	- Jacobian of a coordinate transformation
k	- reduced frequency $\omega b/U$
$\underline{k}_i$	- wave number vector of the i^{th} disturbance (pressure, entropy, etc.)
k_i, ϕ_i, ψ_i	- spherical polar coordinates
M	- Mach number
m	- ratio of normal flow velocities across a shock wave (Section IV and Appendix A)

LIST OF SYMBOLS (Cont'd)

m	- summation index indicating circumferential part of modal designation (Appendix B)
$\underline{n}$	- unit normal vector
P	- static pressure of fluid (Section IV and Appendix A) power spectral function corresponding to p(t)
$p(t)$	- fluctuating static pressure disturbance
$R_{m\mu}(r)$	- modal function for annular duct
R_o	- outer radius of annular duct
$S(k)$	- Sears function modifying the quasi-steady response of an airfoil to a sinusoidal transverse gust
S	- entropy of the fluid
S_i^k	- transfer function for a k-type disturbance upstream of a shock wave generating an i-type downstream disturbance
s	- fluctuating entropy disturbance
t	- time
$\underline{U}$	- flow velocity vector relative to a coordinate system moving with the shock waves (Section IV and Appendix A)
U	- free stream velocity in Section V
$\underline{U}_f$	- phase velocity vector of pressure wave relative to a stationary coordinate system
$\underline{U}_p$	- velocity of propagation of pressure disturbance relative to a coordinate system moving with the shock waves
$\underline{u}$	- fluctuating velocity disturbance vector
$v(t)$	- transverse velocity fluctuation
$V(\omega)$	- power spectral function corresponding to v(t)

LIST OF SYMBOLS (Cont'd)

x	- axial distance downstream of rotor, divided by R_o
α	- angle between rotor velocity vector and the flow velocity vector $\underline{U}$ (Section IV and Appendix A)
α	- angle of incidence of airfoil (Section V)
γ	- ratio of specific heats
$\kappa_{m\mu}$	- Eigenvalue corresponding to mode of annular duct
ϵ	- a factor in equation 5 having a value of one or zero
ϵ	- angle made by blade chord with axial direction (Appendix B)
σ	- angle between flow velocity vector $\underline{U}$ and the shock wave (Section IV and Appendix A)
σ_x, σ_θ	- axial and tangential components of fluctuating lift on blade
ξ, η, X_3	- Cartesian coordinate (ξ normal to the plane of the shock wave)
ρ	- density of the fluid
θ	- angular coordinate in plane parallel to rotor
Φ_{ii}	- spectral function of the i^{th} disturbance
μ, μ'	- summation index indicating radial part of modal designation
$\underline{\Omega}$	- vorticity disturbance vector (Section IV); also angular speed of rotor rotation
ω	- frequency of disturbance relative to an observer moving with the shock wave (Section IV)
ω	- general frequency (radians/second) in Section V

SUBSCRIPTS

m	- circumferential part of modal designation
p	- pressure disturbance

lv	-	the component of the vorticity-associated velocity disturbance normal to the shock wave
s	-	entropy disturbance
t	-	turbulence
°	-	stagnation property
ω	-	spectral component at frequency ω

SUPERSCRIPTS

(′)	-	indicates property downstream of shock wave
p, lv, s	-	same as under subscripts

I INTRODUCTION

The design of axial compressors for low noise output has benefited from a number of studies related to discrete frequency noise (References 1 and 2). By selection of relative numbers of rotor and stator vanes and by judicious use of acoustic absorbing linings within inlet and fan discharge passages, the discrete frequency content of the total noise spectrum can be minimized so that the broadband or continuous spectrum noise has become a source of primary concern. It was observed that this type of noise becomes predominant as the surge line is approached, indicating its close relationship to such diverse phenomena as the turbulence in blade wakes, randomly intermittent separation of boundary layer flow by passing inhomogeneities in the stream, and others. The broadband noise levels caused by interaction of turbulence with rotor-attached shocks and with highly loaded aerodynamic surfaces of a downstream blade row are two aerodynamic noise mechanisms for which basic theories have been constructed.

The primary purpose of the research reported here was to apply these basic theories to the flow geometry and levels of blade loading found in axial compressor fans. In addition, a further purpose was to supply experimental data on unsteady blade response under highly loaded conditions, since current theory necessarily assumes the applicability of thin-airfoil unsteady aerodynamics. This application included a numerical prediction of the broadband noise levels resulting from the two mechanisms. In order to accomplish these purposes, the following immediate research objectives were established:

- To construct an analytical procedure for calculation of the broadband noise produced by interaction of normal inlet turbulence with the rotating shock system produced by a fan at supersonic relative velocities.

- To construct an analytical procedure for calculation of the broadband noise produced by interaction of turbulence with highly loaded aerodynamic surfaces of a downstream blade row.

- To provide experimental data regarding fluctuating surface pressure distributions, establishing deviations from unsteady aerodynamic theory under conditions of high loading.

- To provide a comparative analysis of the relative noise amplitudes to be expected from these aerodynamic mechanisms during operation of a fan or compressor stage.

The approach to these objectives consists of three parts having to do with two general mechanisms of broadband noise. The first mechanism, that of interaction of inlet turbulence with the rotor shock system, is treated purely analytically; the second mechanism, that of interaction of fluctuating upwash with a highly loaded airfoil, is treated both analytically and experimentally.

TURBULENCE-SHOCK INTERACTION (ANALYTICAL)

This branch of aerodynamic acoustics is relatively unfamiliar both to aerodynamicists and to noise specialists, so that close study of the references is required to permit detailed understanding of the developments reported here. According to the theory outlined in References 3 and 4, the interaction of turbulence with a shock wave may be treated in terms of single shear wave components or infinitesimal contributors to the Fourier integral which describes the turbulence spectrum. The results of shock interaction with an arbitrary shear wave must then be integrated over all possible orientations and wavelengths to obtain the total result. Further, although the turbulence can be described in terms of vorticity alone, its interaction implies an energy exchange which creates a more general condition. This more general condition involves the simultaneous existence of pressure, entropy and vorticity waves which have drawn energy from the shock wave during the interaction. Thus, an amplification of the original vorticity is possible, as well as the creation of the propagating pressure waves (aerodynamic noise) from the vorticity or shear waves which, in common with the entropy or temperature waves, do not propagate but merely travel with the steady flow.

Ribner's work (Reference 4), as well as recent work by Lowson (Reference 5), has averaged the production of noise (propagating pressure waves) over all directions of travel of the pressure waves. This leaves much to be desired in terms of noise produced by rotor shock waves in an inlet, since only that noise which propagates parallel to the shock wave can escape upstream. Most of the noise is indeed propagated in this direction, but proper estimates have not yet been made.

An additional factor is the close spacing of the shocks from successive rotor blades which will cause coherent sound to be produced behind adjacent shocks as a single shear wave interacts with them. Retention of directivity of the shear wave and its products was essential if this effect was to be studied.

TURBULENCE-AIRFOIL INTERACTION (ANALYTICAL)

A theory of broadband noise produced by random fluctuating upwash interacting with a downstream blade has been developed by Pratt & Whitney Aircraft in conjunction with an outside firm. This theory follows the linearized aerodynamics of Reference 6 in relating lift fluctuations to downwash and derives the resulting acoustic broadband field. The conclusion was that the noise resulting from any specific upwash spectrum was controlled by the behavior of the Sears function which relates steady and unsteady airfoil aerodynamics to each other. It was desired to explore the implications of this conclusion by numerical studies of the theory with empirical modifications of the theoretical Sears function, especially since there was reason to expect that the Sears function relationship will require modification at large values of blade loading and wave number.

The broadband noise spectrum predicted by this theory was calculated for parameters corresponding to a recent fan design study and the quantitative results of deviations from the Sears unsteady aerodynamics have been explored.

TURBULENCE-AIRFOIL INTERACTION (EXPERIMENTAL)

This experiment, conducted in a high speed cascade tunnel with a single instrumented blade, measured the fluctuating pressure distribution on the airfoil surface acted upon at varying angles of attack by the oscillating wake shed from an upstream cylindrical rod. It was particularly desired to obtain conditions under which the passing vortices of the oscillating wake might trigger separation or otherwise accentuate the random pressure fluctuations on the blade.

The experimental program used the United Aircraft Research Laboratories two-dimensional, high speed cascade tunnel, which receives air from a large pressurized plenum chamber through a rectangular bellmouth and exhausts to the atmosphere. Hot wire instrumentation was used to define the fluctuating upwash velocities received by the test airfoil.

The test airfoil (about 0.05 thickness/chord ratio and 3-inch chord) has a symmetrical (circular arc) cross section, instrumented with ten absolute pressure transducers of 40 kilohertz response. The transducers have a sensing area of 0.012 square inch and are mounted flush with the surface. Their output was studied by statistical correlation techniques to provide data in appropriate form for use with the analysis of the broadband noise field resulting from the interaction of turbulence with a downstream blade row.

II CONCLUSIONS

1. At the high reduced frequency (3.9) of this experiment, the unsteady aerodynamic response of an airfoil to fluctuating upwash was found to remain substantially unchanged as the steady loading was increased from zero to values exceeding stall.

   a) The magnitude of the lift response to an oscillating upwash is greater than that predicted on the basis of the unstalled static lift-curve slope by about 50 percent.

   b) Beyond stall, there is a slight increase in phase lag past that predicted by the Sears theory. This lag is virtually negligible for acoustic purposes.

2. Although the unsteady thin airfoil theories predict stationary oscillating pressure distributions, the measured pressure distributions on the instrumented airfoil exhibit a traveling wave nature.

3. The interaction with rotors of turbulence having intensity compatible with that produced by upstream vanes, struts or splitters can produce broadband noise of substantial power. The effect of increased steady loading on the dynamic response of the blades is not great enough to affect this conclusion, based on the single-frequency data of the experiment.

4. The interaction of turbulence with the rotating system of shock waves from a supersonic rotor can generate a broadband power spectral density in roughly the same range as that from interaction with the downstream rotor blades.

5. Significant characteristics of shock/turbulence interaction noise are as follows:

   a) The acoustic pressure increases linearly with shock strength for weak shocks, then remains substantially constant with further increases in shock strength. The noise is highly directional, tending to travel upstream and parallel to the moving shock when viewed from rotating coordinates.

   b) At a supersonic design speed, variation of pressure ratio would not be expected to cause significant changes in shock strength or orientation, hence little change in broadband noise level should result.

   c) At supersonic speeds below the design condition, increasing pressure ratio reduces the mass flow and hence the Mach number at which the turbulence approaches the shock system. For relatively weak shocks, calculations show that the noise level will increase with pressure ratio.

III RECOMMENDATIONS

1. Extended experiments should be made over a wider range of reduced frequencies on the unsteady sinusoidal gust response of heavily loaded airfoils. The effects of chordwise distribution of unsteady pressure should be explored.

2. The significantly different behavior of shock/turbulence interaction noise for low and high values of the shock normal Mach number requires for its study an experimental flow geometry with minimum spanwise variation. This requirement is in common with the general principle of avoiding multiple aerodynamic noise mechanisms. A noise facility having this feature of uniform flow conditions, yet possessing as far as possible the aerodynamic passage of a normal compressor stage, should be used for such investigations.

IV THE GENERATION OF BROADBAND NOISE BY THE INTERACTION OF TURBULENCE WITH SHOCK WAVES

BACKGROUND

The present work is concerned with the generation of broadband noise by the interaction of turbulence with several shocks. This condition exists in front of a supersonic compressor where the turbulent eddies generated in the inlet are convected through the system of rotating shocks generated by the rotor. Since the axial Mach number is usually less than one in a supersonic compressor, the shock waves will propagate upstream of the rotor and some of the noise produced by shock-turbulence interaction will escape from the inlet of the compressor.

The interaction of turbulence with shock waves has been studied by several authors (notably References 3, 4, 5, 7, 8, and 9). All of these investigations considered one shock wave interacting with one or more types of elementary disturbances. The results of these investigations show that three independent types of disturbances (entropy, vorticity, and pressure) are generated downstream of the shock wave as a result of the interaction of each type of disturbance with the shock wave. The pressure disturbance is of two types: a near field which decays exponentially with distance and a far field for which the wave amplitude is constant with distance. (In this work the near field is ignored.) It has also been shown that the intensity of the pressure disturbance is greatest for waves propagating nearly parallel to the shock wave.

In order to estimate the noise produced by shock-turbulence interaction in front of a supersonic rotor, one must consider the interaction with several shocks. For the purpose of this investigation, the scale of turbulence was assumed to be such that a system of three shocks (as shown in Figure 1) must be considered. For simplicity, the flow model chosen contains parallel plane oblique shock waves of equal strength. The flow is assumed to be turned isentropically between the shocks so that the flow into the three shocks continues in the same direction. These assumptions are nearly satisfied in the region upstream of the rotor where the shocks are relatively weak. Figure 1 is helpful in clarifying the flow model.

MATHEMATICAL ANALYSIS

Since the upstream disturbance is assumed to be random, one can only obtain statistical knowledge of the downstream disturbances. Thus the spectral function of the pressure waves (mean square pressure amplitude versus wave number) will be found in terms of the spectral function of the upstream turbulence (mean square amplitude of the velocity fluctuation versus wave number). From the spectral function, the mean square of the pressure fluctuations and the acoustic energy flux can be found by integrations over the appropriate wave numbers as shown in equations 1, 2, and 3.

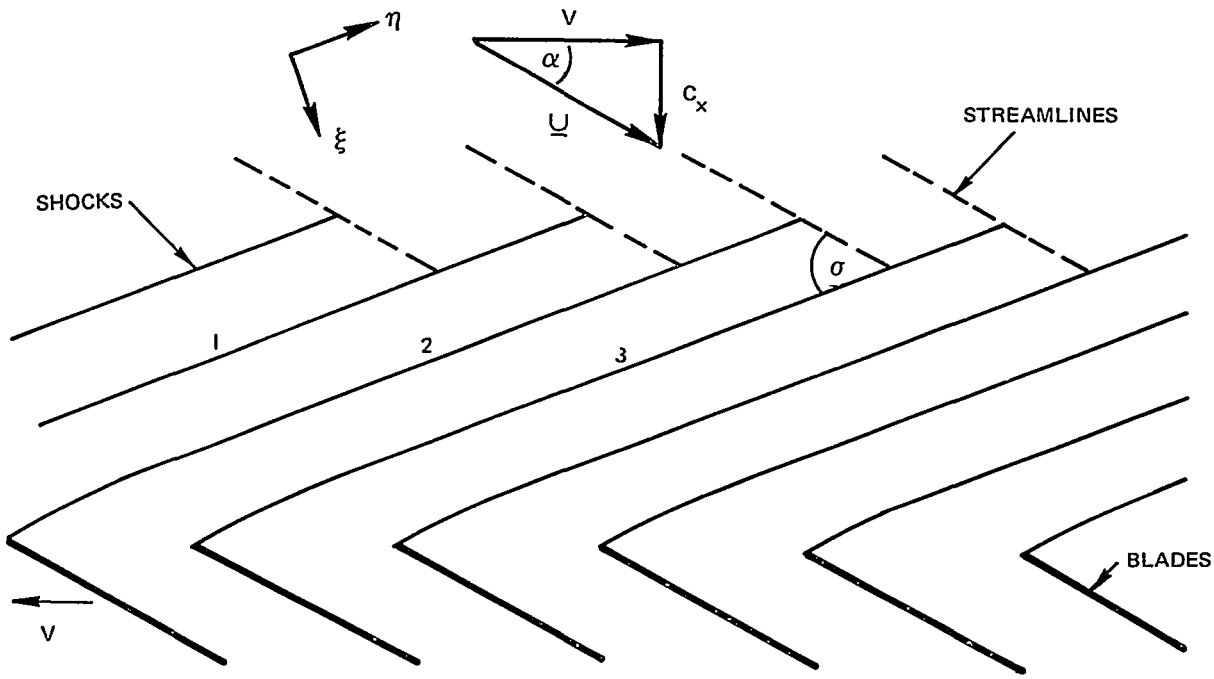

Figure 1 Flow Model

$$\overline{\left(\frac{p'}{P'}\right)^2} = \int \Phi'_{pp}\,(\underline{k}'_p)\; d\underline{k}'_p \tag{1}$$

$$I'_p = \int\int e'_p\; \underline{U}'_p \cdot \underline{n}\;\; d\underline{k}'_p\; dA \tag{2}$$

where e'_p is the acoustic energy density of a quasi-plane wave relative to a stationary coordinate system,

$$e'_p = \frac{P'}{\gamma_{a'}}\;\; U'_f\;\; \Phi'_{pp}\,(\underline{k}'_p) \tag{3}$$

Here Φ'_{pp} is the spectral function of the pressure disturbance, $\underline{k}'_p$ is the wave number vector of the pressure wave, P' and a' are the static pressure and sound speed downstream of the shock, $\underline{U}_f = (a + \underline{c}\cdot\underline{k}_p/k_p)\,\underline{k}_p/k_p$ (a is the sound speed, $\underline{c}$ is the fluid velocity relative to a stationary observer) is the phase velocity of a wave front relative to a stationary coordinate system, $\underline{n}$ is the unit normal to the surface element dA and $\underline{U}_p = \underline{U} + a\underline{k}_p/k_p$ ($\underline{U}$ is the fluid velocity relative to an observer moving with element dA) is the propagational velocity of the wave front relative to a coordinate system fixed to dA. (It is assumed that geometric acoustics is applicable in calculating the acoustic energy flux).

The theory relating disturbances upstream of a shock wave to downstream disturbances has been done by several authors. The results of Kerrebrock (Reference 7) are used here. Since this reference is an unpublished Ph. D. thesis and not readily available, a summary of it appears in Appendix A.

In the present problem, turbulence (a packet of shear waves) is assumed to be convected into shocks 1, 2 and 3. In order to determine the resulting pressure disturbance downstream of shock 3, one must consider single, double and triple interactions. Figure 2 shows the possible combinations of interactions for pressure waves to be created by shear (vorticity) waves. The vorticity and entropy waves are convected by the flow and thus follow streamlines. The pressure waves propagate with a velocity $\underline{U}_p = \underline{U} + a\underline{k}_p/k_p$ relative to the shock wave.

INTERACTIONS

SHOCK	SINGLE	DOUBLE			TRIPLE								
1					V	V	V	V	V	V	V	V	V
2		V	V	V	P	P	P	S	S	S	V	V	V
3	V	P	S	V	P	S	V	P	S	V	P	S	V
	P	P	P	P	P	P	P	P	P	P	P	P	P

V=VORTICITY

S=ENTROPY

P=PRESSURE

Figure 2 Combinations of Interactions of Pressure Waves Caused by Vorticity Waves

Consider a wave-like disturbance with a given wave front orientation upstream of a shock wave; three independent waves are formed downstream of the shock. For steady flow, the inclination of the downstream wave fronts is such that the frequency (ω) of the upstream and downstream waves are equal for an observer fixed on the shock wave. For propagating waves (pressure) $\omega = \underline{k}_p \cdot \underline{U} + ak_p$ and for non-propagating waves (vorticity and entropy) $\omega = \underline{k} \cdot \underline{U}$. The relations between the amplitudes of the upstream and downstream waves are determined by using a perturbation technique with the one-dimensional shock relations. These relations are developed in Appendix A. As the waves pass between shocks, it is assumed that the amplitudes of the waves do not change. However, since the flow velocity and sound speed do change between the shocks due to the isentropic turning, one must account for the change in inclination of the wave fronts. This change in inclination must provide that the frequency remains constant relative to a coordinate system fixed to the shocks. Thus, one has for propagating waves

$$\omega = \underline{k}_p \cdot \underline{U} + ak_p = \text{constant}$$

and for non-propagating waves

$$\omega = \underline{k} \cdot \underline{U} = \text{constant}$$

Using the above assumptions and following the analysis of Appendix A, one obtains equation 4 for the spectral function of pressure disturbances downstream of the third shock.

$$\Phi'_{pp}\ (k_v,\phi'_p,\psi'_p,\eta) = B(\phi'_p)\ E\ (k_v)\ F\ (\phi'_p,\psi'_p,\eta) \Big/ 2\pi\, U_1^2$$

where

$$B(\phi'_p) = \frac{\frac{1}{m}\left(1 + \frac{\cos(\phi'_p)}{M_1}\right) \sin^3(\phi'_p)}{\left(\left(\frac{1}{m}\left(\cos(\phi'_p) + \frac{1}{M'_1}\right)\right)^2 + \sin^2(\phi'_p)\right)^{5/2}} \tag{4}$$

Here the spectral function is a function of the wave number of the upstream vorticity wave number (k_v), the inclination of the downstream pressure wave fronts (φ'_p and ψ'_p) and the position on the shock (η). In equation 4, E (k_v) is the energy-spectrum function of the upstream turbulence and F (ϕ'_p, ψ'_p, η) is a linear combination of the transfer functions discussed in Appendix and shown in equation 5.

$$\begin{aligned}
F(\phi'_p, \psi'_p, \eta) &= \epsilon_1 \left|S^{1v}_p\right|^2_3 + \epsilon_2 \left|S^{1v}_p\right|^2_2 \left|S^{p}_p\right|^2_3 \left(\frac{P'}{P}\right)^2 + \epsilon_3 \left|S^{1v}_s\right|^2_2 \left|S^{s}_p\right|^2_3 + \epsilon_4 \left|S^{1v}_{1v}\right|^2_2 \left|S^{1v}_p\right|^2_3 \left(\frac{U'_1}{U_1}\right)^2 \\
&+ \left|S^{1v}_p\right|^2_1 \left(\frac{P'}{P}\right)^2 \left\{\epsilon_5 \left|S^{p}_p\right|^2_2 \left|S^{p}_p\right|^2_3 \left(\frac{P'}{P}\right)^2 + \epsilon_6 \left|S^{p}_s\right|^2_2 \left|S^{s}_p\right|^2_3 + \epsilon_7 \left|S^{p}_{1v}\right|^2_2 \left|S^{1v}_p\right|^2_3 \left(\frac{U'_1}{U_1}\right)^2\right\} \\
&+ \left|S^{1v}_s\right|^2_1 \left\{\epsilon_8 \left|S^{s}_p\right|^2_2 \left|S^{p}_p\right|^2_3 \left(\frac{P'}{P}\right)^2 + \epsilon_9 \left|S^{s}_s\right|^2_2 \left|S^{s}_p\right|^2_3 + \epsilon_{10} \left|S^{s}_{1v}\right|^2_2 \left|S^{1v}_p\right|^2_3 \left(\frac{U'_1}{U_1}\right)^2\right\} \\
&+ \left|S^{1v}_{1v}\right|^2_1 \left(\frac{U'_1}{U_1}\right)^2 \left\{\epsilon_{11} \left|S^{1v}_p\right|^2_2 \left|S^{p}_p\right|^2_3 \left(\frac{P'}{P}\right)^2 + \epsilon_{12} \left|S^{1v}_s\right|^2_2 \left|S^{s}_p\right|^2_3 \right. \\
&\left. + \epsilon_{13} \left|S^{1v}_{1v}\right|^2_2 \left|S^{1v}_p\right|^2_3 \left(\frac{U'_1}{U_1}\right)^2\right\}
\end{aligned} \tag{5}$$

The ϵ_i's are either 1 or 0 depending on whether or not the particular combination of interactions is possible. For convecting disturbances, the ϵ_i's are a function only of position on the shock. For pressure disturbances, the ϵ_i's are a function of the direction associated with the wave propagation velocity ($\underline{U}_p$) since the pressure waves upstream of shock 3 may escape before striking shock 3.

Following Ribner (Reference 9) the ratio of the acoustic energy flux to the flux of the kinetic energy of turbulence can be found since the latter can be found from equation 6 and 7.

$$I_t = \int e_t \underline{U} \cdot \underline{n}\, dA \tag{6}$$

where, for isotropic turbulence,

$$e_{t_v} = \frac{5}{2}\rho\,\overline{u_{1v}^2} = \frac{5}{3}\rho\int E(k_v)\,dk_v \tag{7}$$

Thus, by taking the area in equations 2 and 6 as the shock area, the ratio of the acoustic energy flux to the flux of the kinetic energy of turbulence becomes equation 8.

$$\frac{I'_p}{I_t} = \frac{0.3}{\pi M_1^{\,3}\gamma^2}\,\frac{P'}{P}\,\frac{a'}{a}\int_0^1\int_0^{2\pi}\int_{\phi'_{p_L}}^{\phi'_{pcr}} M'_f\,M'_{1p}\,B(\phi'_p)\,F(\phi'_p,\psi'_p,\eta)\,d\phi'_p\,d\psi'_p\,d\bar{\eta} \tag{8}$$

See equation 4 for definition of $B(\phi'_p)$.

The upper limit of integration for ϕ'_p is the critical angle or the maximum value of ϕ'_p for which k'_{1p} is real (i.e., for larger values of ϕ'_p the pressure disturbance decays exponentially with ξ). Physically this occurs when the pressure disturbance created at the shock wave propagates into the shock. The limit condition (equation 9) is:

$$U'_{p1} = U'_1 + a'\frac{k'_{1p}}{k'_p} = 0$$

or

$$\cos(\phi'_{pcr}) = -M'_1 \tag{9}$$

The lower limit of integration for ϕ'_p in this investigation is the minimum angle of ϕ'_p for which the pressure disturbance will propagate upstream (ie., toward the inlet of the compressor). The limit condition is

$$U'p \text{ axial} = 0.$$

This condition results in solving the equation 10 for ϕ'_{pL}.

$$\frac{M'_1 + \cos(\phi'_{pL})}{M'_2 + \sin(\phi'_{pL})\sin(\psi'_p)} = \tan(\sigma - \alpha) \tag{10}$$

RESULTS

The spectral function of the pressure disturbance (equation 4) is shown to be a function of k_v, ϕ'_p, ψ'_p and η. The dependence on k_v is entirely due to the energy-spectrum function $E(k_v)$ and the dependence on ψ'_p and η is not explicit as it arises only from the fact that the shock waves are assumed to be of finite extent (ie., some of the pressure waves upstream of a shock wave may escape before striking the shock wave making some interactions impossible). If one considers, for the moment, that the shocks are of infinite extent, the effects of the number of shock waves, the various interactions, and the shock strengths on the spectral function of the pressure disturbance can be found as a function of shock strength and the angle ϕ'_p. Integrating equation 4 over ψ'_p (0 to 2π) and dropping the η using the above assumptions one obtains,

$$\Phi'_{pp}(k_v, \phi'_p) \frac{U_1^2}{E(k_v)} = B(\phi'_p)\ F(\phi'_p) \qquad (11)$$

See equation 4 for definition of $B(\phi'_p)$.

Equation 11 has been evaluated for four types of interactions:

1. One shock wave with a vorticity disturbance upstream of the shock. (ϵ_1 only non-zero ϵ_i in equation 5)

2. Two shock waves with a vorticity disturbance upstream of the first shock wave, ignoring pressure disturbance upstream of the second shock wave. (ϵ_3 and ϵ_4 only non-zero ϵ_i in equation 5)

3. Three shock waves with a vorticity disturbance upstream of the first shock wave, ignoring pressure disturbances upstream of the second and third shock waves. (ϵ_9, ϵ_{10}, ϵ_{12}, and ϵ_{13} only non-zero ϵ_i in equation 5)

4. Same as 2 except that the pressure disturbance upstream of the second shock wave is not ignored. (ϵ_2, ϵ_3 and ϵ_4 only non-zero ϵ_i in equation 5)

Comparison of the numerical results for the various interactions shows that the spectral function resulting from an upstream pressure disturbance has a magnitude much greater than from vorticity and entropy disturbances. The spectral function for any type of interaction had large values only for angles near the critical angle. In the case of stronger shocks, the spectral function was significant over a wider range of the angle ϕ'_p. The above results become important when considering shocks of finite extent. As ϕ'_p is decreased from ϕ'_{pcr}, the vector U'_p (velocity of propagation of the pressure disturbance) tips away from the plane of the shock wave toward the next shock wave. Thus, as the shock strength increases, more pressure waves of significant amplitude will interact with the next shock wave, rather than escape between the shocks.

The flux of acoustic energy in the forward axial direction per unit area was found using equation 2, which is valid for quasi-plane waves. This becomes equation 12.

$$i'_p = \frac{I'_p}{A} = \frac{9}{4\pi} \frac{P'a'}{\gamma} \frac{\overline{Mcx}}{M_1} \left(\frac{\overline{u_{iv}}}{U_1}\right)^2 \int_0^1 \int_0^{2\pi} \int_{\phi'_{pL}}^{\phi'_{pcr}} M'_f M'_{1_{p'}} B(\phi'_p)\, F(\phi'_p, \psi'_p, \eta) d\phi'_p\, d\psi'_p\, d\bar{\eta} \qquad (12)$$

(see equation 4 for definition of B (ϕ'_p) where A is the area between the shocks measured perpendicular to the axial direction. This result was converted to decibels for various flow conditions using equation 13.

$$db = 10 \log_{10}(i'_p/i_o),\ (i_o = 10^{-9}\ \text{erg/sec-cm}^2) \qquad (13)$$

It can be seen from Figure 3 that the intensity of the noise increases very rapidly to very high levels as the upstream Mach number normal to the shock wave is increased.

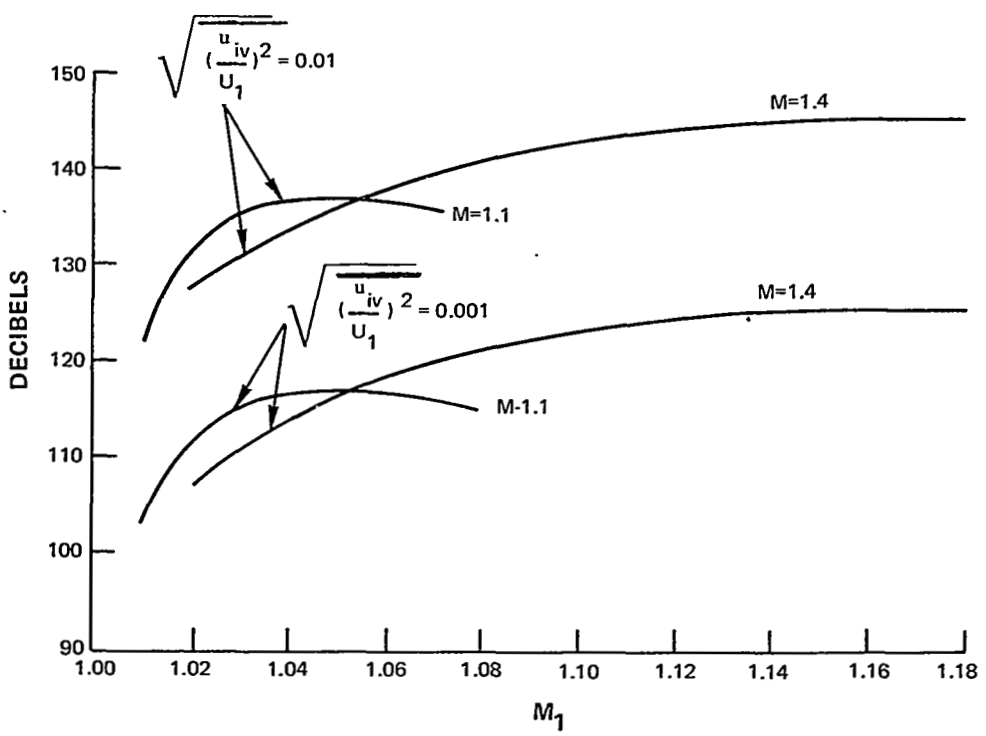

Figure 3 Relative Noise Level Versus Upstream Normal Mach Number

The ratio of the acoustic energy flux to the flux of the kinetic energy of turbulence was found for various flow conditions using equation 8. These results are compared to the results of Ribner (Reference 9) in Figure 4. Ribner's results apply to the interaction of turbulence with one plane normal shock wave, whereas the present results are for the interaction of turbulence with three oblique shock waves. As expected, the present results predict higher values for this ratio.

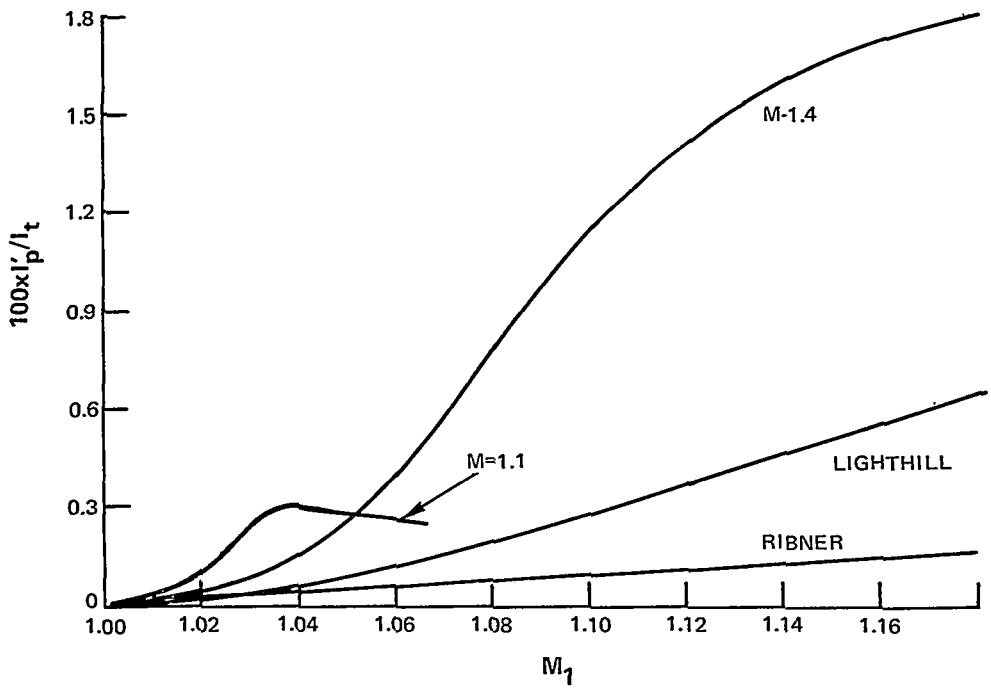

Figure 4 Ratio of Acoustic Energy Flux to Turbulent Energy Flux Versus the Upstream Normal Mach Number

V THE GENERATION OF BROADBAND NOISE BY THE INTERACTIONS OF TURBULENCE WITH A DOWNSTREAM BLADE

BACKGROUND

Turbulent interaction with an airfoil has been treated as a source of broadband noise in several connections, particularly in terms of the impingement on a stator by rotor wake turbulence and of the interaction by a rotor blade with inlet turbulence. Both are potentially important aerodynamic noise mechanisms, and both require the application of some form of unsteady flow theory to obtain the fluctuating force on the aerodynamic surface. The most immediately applicable theory is that developed by Sears in Reference 11, in which assumptions are made which include a sufficiently low loading to secure a linear dependence of load on the upwash velocity. The upwash is assumed to vary sinusoidally in the streamwise direction, and to be stationary in a set of coordinates which move at the free stream velocity.

The upwash then induces a fluctuation of bound vorticity in the blade, corresponding to a chordwise distribution of stream velocity perturbation which drifts with the stream as the sinusoidal gust passes. The Kutta condition at the trailing edge of the airfoil constitutes a boundary condition which requires for its satisfaction that a fluctuating vorticity be shed as a wake downstream of the airfoil. The Sears theory then proceeds to find a fluctuating pressure distribution on the airfoil chord which rises and falls as upwash peaks come and go, but retains the shape of the steady-state pressure distribution.

The fluctuating lift, the chordwise integral of this pressure distribution, follows the upwash fluctuations as they strike the leading edge of the airfoil; at very low frequencies, its maximum value occurs when the maximum upwash passes the leading edge. At higher frequencies, the lift lags this event by an increasing amount eventually reaching one-eighth of the period of oscillation, meanwhile decreasing in magnitude inversely as the square root of the frequency.

A similar theory has been developed by Horlock (Reference 12) for lift fluctuations resulting from periodic variations in the stream velocity when the airfoil is at some angle of inclination to the stream. The gust component transverse to the chord constitutes a Sears-type gust with corresponding lift fluctuations, while the chordwise component of the gust creates a fluctuating interaction with the bound vorticity already existing by virtue of the steady lift. The net result is an unsteady lift function which behaves closely similar to the Sears function as the gust frequency increases.

The principal limitation of these theories was considered to lie in their failure to recognize unsteady aerodynamic stall phenomena at high loading conditions. Accordingly, it was proposed to construct an empirical replacement for the Sears theory relationship by means of experiments on a highly loaded airfoil subjected to the sinusoidal wake of a circular cylinder.

It is worthy of comment that the Sears theory assumes a sinusoidal upwash interacting with the thin airfoil and that the Karman street is such a flow. The Sears theory ignores any accompanying sinusoidal variation of inflow (considered separately by the Horlock theory) in spite of the requirements of continuity. Application of the continuity and irrotationality

conditions shows that the variations of inflow must lead the crossflow by a quarter cycle, that their amplitudes are equal, and that both amplitudes must (asymptotically) diminish exponentially with transverse distance from the center of symmetry.

The analytical prediction of broadband noise resulting from the impingement of a turbulent airflow on a blade is based on the initial development of an expansion for the instantaneous pressure at a point in the acoustic field, in terms of the instantaneous force exerted on the air by the interaction of an airfoil with the turbulent airflow. This expression is used to generate a closely related, parallel expression for the power spectrum of the acoustic pressure in terms of the power spectrum of the force fluctuation.

The development of this power spectral relationship involves considering the statistical correlation (autocorrelation) of the fluctuating force with its value at a slightly different time, averaged over all such time differences. This averaging process eliminates the difference in phase associated with frequency, retaining in the power spectral relationship only the magnitude of the fluctuating force. In terms of the linearized aerodynamics used to obtain the force fluctuation from the turbulent gust which strikes the airfoil, only the magnitude of the Sears function affects the power spectral relationship; the frequency-dependent phase lag is immaterial.

The interaction of blade wake turbulence with a downstream blade has been analyzed in Reference 13 in terms of this power spectral relationship, and a typical broadband spectrum is shown in Figure 5. An abbreviated treatment paralleling that of Reference 13 is given in Appendix B. The interaction in this case takes place on a rotor blade, and assumes a random force per unit span having a time dependence g(t) leading to the power spectral function

$$G(\omega) = \int_{-\infty}^{\infty} e^{i\omega(t_1 - t_2)} \, <[g(t_1)]\ [g(t_2)]^* > d(t_1 - t_2) \tag{14}$$

If the force g(t) is created by upwash velocity v(t) in a manner consistent with the Sears unsteady airfoil theory, their Fourier transforms $g(\omega)$ and $v(\omega)$ are related by

$$g(\omega) = \frac{dC_L}{d\alpha} \ \rho U b \ S(k)\, v(\omega) \tag{15}$$

in which S(k) is the Sears function. Then, if $V(\omega)$ is the power spectral density of the upwash velocity fluctuation,

$$G(\omega) = \left(\frac{dC_L}{d\alpha} \ \rho \ \frac{Ub}{G_0}\right)^2 \ |S(k)|^2 \ V(\omega) \tag{16}$$

Here, G_o is a normalization factor such that

$$\int_{-\infty}^{\infty} G(\omega)\, d\omega = 1 \tag{17}$$

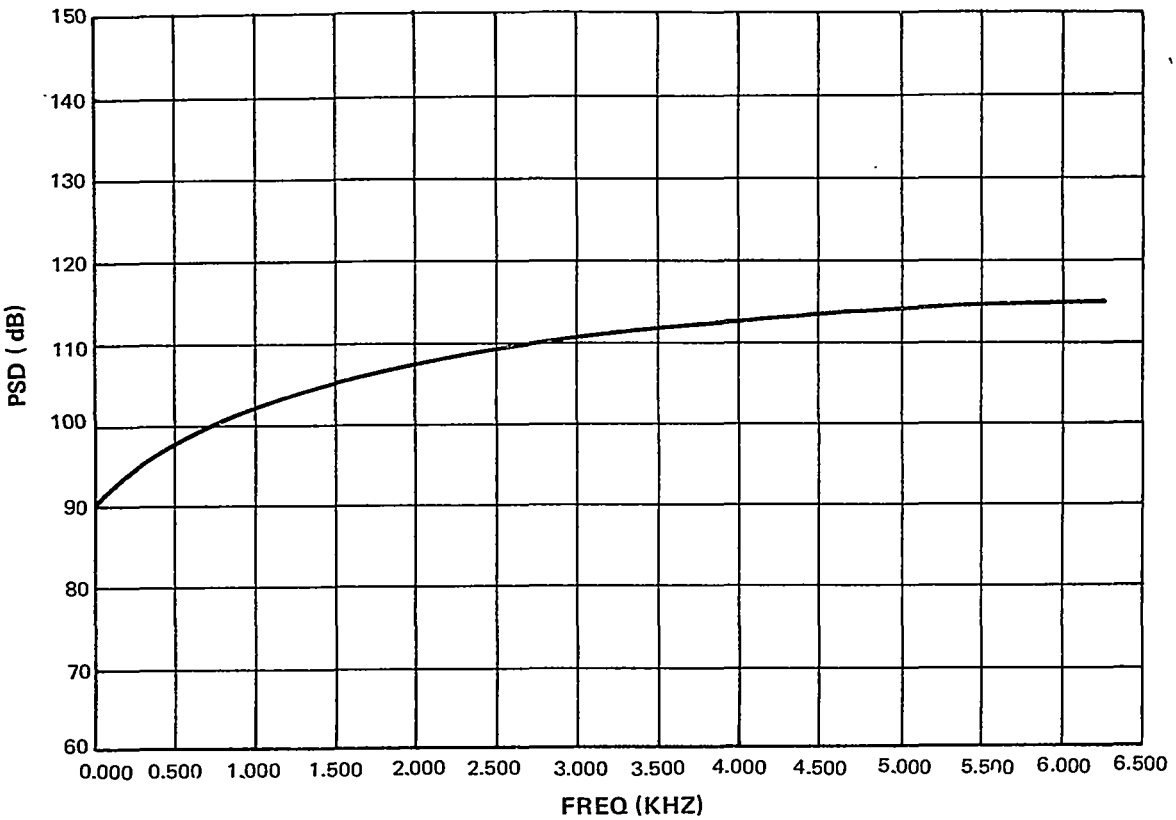

Figure 5 Broadband Noise Spectrum From Turbulence/Blade Interaction

EXPERIMENTAL APPROACH

The choice of experimental parameters was dictated to some extent by the existing wind tunnel and model described in the introduction. Four parameters entered interdependently into the design of an upwash - generating cylinder-blade configuration consistent with the desired measurements: the Reynolds number based on cylinder diameter, the free stream Mach number, the reduced frequency based on blade semichord, and the Karman-shedding reduced frequency based on cylinder diameter, which becomes 1.25 for Reynolds numbers greater than 300.

The airfoil semi-chord of 1.5 inches was set by the existing airfoil. Limits on the Mach number arise from two sources. First, a Mach number greater than 0.20 was required so that the pressure transducers would have adequate signal to noise ratios. Second, a Mach number less than 0.40 was somewhat arbitrarily selected to minimize the non-linear compressibility effects inherent in the hot-wire anemometer measurements of the velocity fluctuations in the flow field. Thus, the experimental bounds on the velocity were 220 and 450 ft/sec.

With semi-chord fixed and velocity bounded, the frequency range required to achieve a reduced frequency of 3.0 was found to be from 840 to 1720 cps. The frequency at which vortices are shed from a cylinder is a known function of Reynolds number. For a Reynolds number greater than 300 the shedding reduced frequency based on cylinder diameter is approximately constant at 1.25. This value, together with the required frequency range and practical velocity range, both given above, determined the cylinder diameters. These diameters in turn establish the actual Reynolds number range. If the resulting Reynolds number are sub-critical (less than 4×10^5), the cylinder geometry represents an acceptable configuration for additional study. Based on these concepts, two cylinders were selected to be tested further at a Mach number of 0.25, having diameters of 1.12 and 2.25 inches.

Experimental evidence shows that when the Reynolds number is greater than 300 the vortex shedding from a cylinder is "irregular"; i.e., a predominant frequency is more or less random. Since tests run at lower Reynolds number than 300 would result in a prohibitively small vertical separation distance between the rows of shed vortices, it was necessary to accept this deficiency.

The next problem considered was the detailed measurements of the fluctuating flow field downstream of the cylinder. Sears' theory assumes the existence of a uniform transverse sinusoidally varying gust field in which an airfoil is immersed. To simulate the model analyzed by Sears, it would be necessary to produce the disturbance in the infinite free stream upstream of the airfoil, and to maintain a spatial and timewise invariance of the disturbance that could be measured at a known distance far upstream of the airfoil. However, in the actual experiment, with horizontal and vertical gradients in the fluctuation amplitude, it is necessary to make these measurements near the airfoil, with the added constraint that the measurements do not disturb the flow over the airfoil. In view of these requirements, it was decided to measure the unsteady flow characteristics at the airfoil location, but with the airfoil removed, to simulate a "free stream" measurement. Simultaneously, measurements of the pressure fluctuation on the cylinder were made to establish a phase angle between the upstream and downstream disturbances. Later in the experiment, the hot wire probe was removed and the unsteady airfoil pressures were measured simultaneously with the fluctuating pressure on the cylinder. The relative phase angle, measured earlier, was then used to infer the "free stream" conditions approaching the airfoil.

The fluctuating flow field was generated by mounting a cylinder in the forward portion of the test section. The cylinder contained a Pitran absolute pressure transducer with a 3/16 inch diameter active surface. Since the Pitran gage was limited to pressures of 10 inches of water, it was necessary to locate the static pressure tap at 45 degrees to the airstream in order to maximize the ratio of fluctuating pressure to static pressure and still stay within the linear range of the gage.

Velocity fluctuations were obtained with two DISA hot-wire constant temperature anemometers. These were used in conjunction with a pair of DISA type 55D10 linearizers and two DISA filters. The crossed wire probes, type 55A32, were calibrated without the cylinder and, by using the linearizers, adjusted for identical linear outputs from each wire versus velocity. The frequency response capability of the system was in excess of 20 kc, well beyond the range of interest in this program. In addition, it was possible to filter the upper and lower ends of the hot wire frequency response in order to enhance the signal being sought and to limit the measurement to the fluctuating velocities.

A survey of the wake behind a fixed cylinder was then made to establish whether or not a discrete frequency could be observed. A small region several diameters downstream and above (or below) the cylinders existed with discrete frequencies of sufficient signal to noise ratios to approximate the desired sinusoidal flow field. On the basis of these tests, the two cylinders were positioned upstream of the fixed airfoil location. These positions were selected individually for each cylinder and represent the points at which the signal to noise ratios were greatest and where discrete frequencies on both wires could be readily observed on an oscilloscope. The wake of the smaller cylinder was more turbulent than that of the larger cylinder, but the discrete velocity fluctuations were of considerably greater magnitude. The turbulent wake of the larger cylinder was broader than that experienced with the smaller cylinder and sizeable discrete velocity fluctuations did not extend as far above and below the cylinder.

This limitation on the region of suitable airfoil positions relative to the large cylinder made it necessary to place the airfoil within 2.35 diameters of the cylinder. Many investigators have found that any object downstream of the cylinder can have a disruptive influence on the shedding phenomenon if it is close enough to the cylinder. Hence, it is not surprising that the data for this cylinder suffered a 25 percent frequency shift and an unknown shift in amplitude (unknown because no hot wire measurements were made with the airfoil installed). Hence, these data were not used in this study. One possible explanation for this shift in frequency is a strong decrease in spanwise correlation of the shedding process reported in the literature as Reynolds number approaches the critical value (which is nominally 4.5×10^5 but which can vary widely depending on tunnel conditions). No significant frequency shift was observed for the smaller cylinder, and it was assumed that the results were valid.

The instrumented airfoil discussed briefly in a preceding section contained ten miniature (1/8 inch diameter) Sensotec pressure transducers. These transducers were calibrated for temperature and pressure and, although "temperature compensated", are extremely sensitive to temperature variations. Temperature compensation in the sense used by the manufacturer means that the pressure sensitivity was constant at any temperature within a specified range. Thus, it was impossible to use these transducers to obtain the static pressure distribution (DC portion of output) around the airfoil without introducing additional equipment to measure transient temperature distributions. To avoid this added complication, the transducers were used to obtain only the fluctuating (AC portion of output) pressures. The tunnel was run at an operating condition for several minutes to allow the airfoil to assume a static temperature distribution which was assumed constant over the few seconds when unsteady data were taken. Static pressure distributions at various angles of attack were obtained later in the program using conventional static pressure taps and a manometer board.

The wind tunnel free stream velocity upstream of the cylinder was set to within 1 ft/sec by using an inclined manometer which could be read to within 0.1 inch of water. All other data taken during the course of this program were acquired and recorded using the WISARD (Wide-Band System for Acquiring and Recording Data). Briefly, the output signals were conditioned and amplified for recording at 60 inches/sec on a variable speed FM tape recorder. After the tests were completed, the FM tapes were played back at 1 7/8 inches/sec to increase the frequency resolution. The analog signal was converted to a digital form compatible with the UNIVAC 1108 digital computer and existing software programs.

The data acquired in this study consisted of FM tapes of hot-wire output signals taken concurrently with the Pitran pressure transducer for each of the two cylinders. These data were taken in the absence of the airfoil at a point corresponding to the leading edge of the airfoil at zero angle of attack and several other positions up and downstream of that point. Later, with the hot wire equipment removed, transient pressure measurements over the airfoil were made for several airfoil angles of attack. This was done for each cylinder and again recorded simultaneously with the static pressure output of the Pitran pressure transducer.

Steady-state tests were conducted with the dynamic pressure transducers replaced by conventional static surface taps. Fourteen taps were placed on one surface, and a single tap was placed on the other surface to check symmetry. The tests were run for both positive and negative angles of attack up to 16 degrees, and the pressure difference across the airfoil was synthesized from the single surface pressures. The pressures were integrated to yield both the lift coefficient and the moment coefficient about the quarter chord. The results are plotted in Figure 6, and it is seen that steady-state stall occurs at an angle of incidence of about 8 degrees.

An objective of this study was to make an experimental measurement of the unsteady lift which could be used to obtain the Sears function at the frequency of the fluctuating flow. This was done by integrating the chordwise pressure difference distribution at a large number of sequential instants of time, covering at least 25 cycles of the fluctuation. The integration was performed using a simple trapezoidal rule, with a parabolic extrapolation to the leading edge, and a zero pressure condition at the trailing edge. This yielded the lift coefficient versus time for each angle of attack.

Despite the limited number of chordwise pressure transducers and the presence of background noise in the velocity fluctuations, the waveform was found to be relatively noise free. Fourier analysis of this signal resulted in Fourier coefficients with a single peak amplitude fifty times greater than the noise level ($\log_{10}[\text{noise}] \approx -2.5$), four times greater than any other peak, and twenty times greater than its second harmonic. Similar analysis of the fluctuating static pressure on the cylinder resulted in a very similar spectrum.

The phasing of the unsteady lift relative to the vertical velocity fluctuation at the midchord was established (as were the individual pressures) by referring both measurements to the fluctuating static pressure on the cylinder. The phase angle between the lift and velocity vectors was established by plotting the phase angles between lift and cylinder pressure and between velocity and cylinder pressure on the same polar plot. The desired phase angle is the angle between the lift and velocity vectors. The magnitude of the unsteady lift was obtained by averaging the maxima and minima of the time varying lift coefficient.

The conversion of the unsteady lift coefficient to an equivalent Sears function vector in the phase plane (including the effects of horizontal flow fluctuations) has been described in Appendix C. The unsteady lift coefficient was shown to be

$$C_L = \frac{2\pi v}{U} \left[S(k) + \frac{u\alpha}{v} i\, T(k) \right] \qquad (18)$$

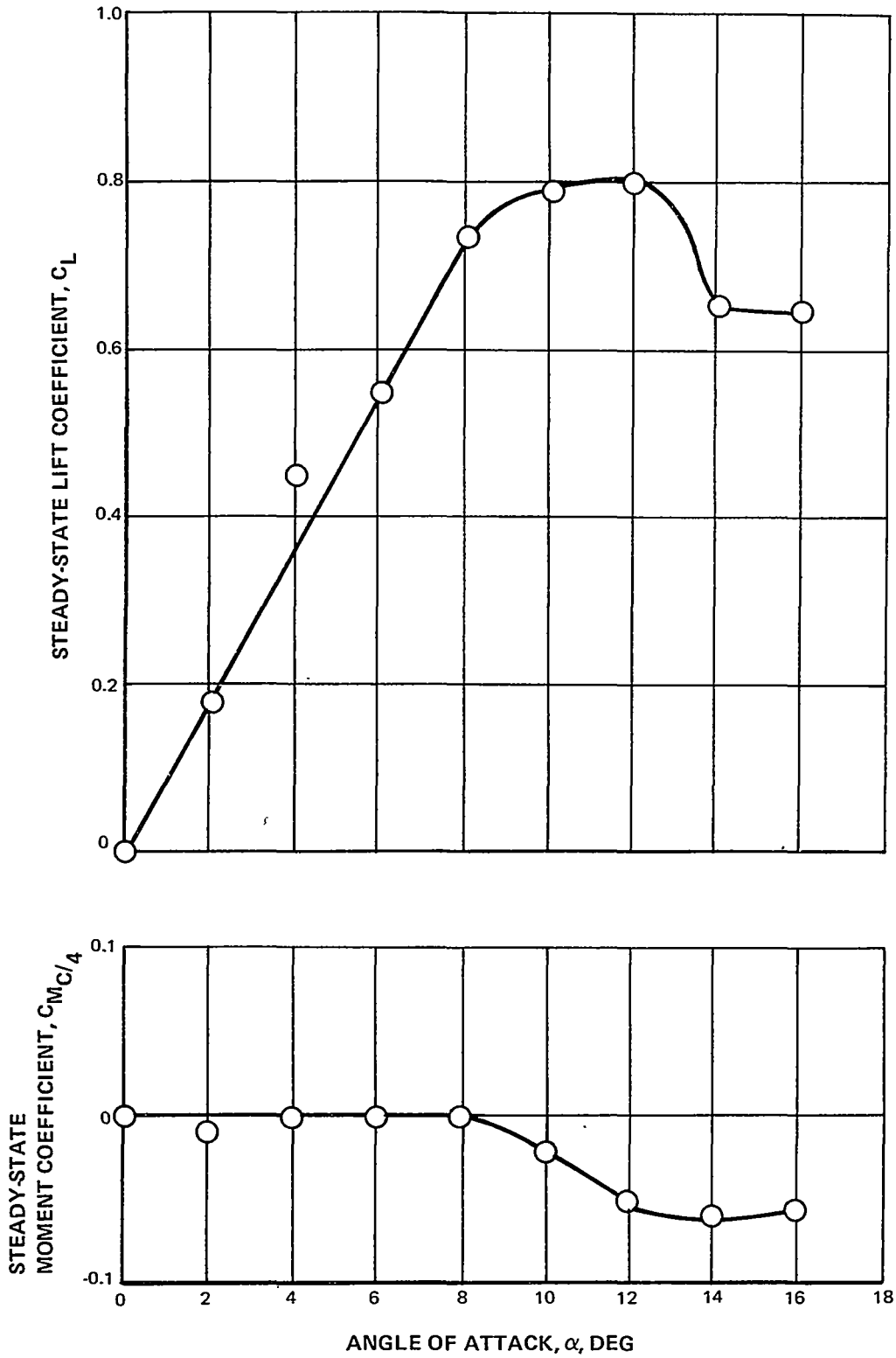

Figure 6 Steady State Blade Characteristics, M = 0.25

Since horizontal flow fluctuations do not contribute to unsteady lift at zero angle of attack, it can be seen that

$$S(k) = \frac{U}{2\pi v} C_L \tag{19}$$

at zero incidence. At the various angles of attack tested, the measured lift coefficients were multiplied by $U/2\pi v$ to obtain the variation in S(k) corresponding to variations in loading. These data are shown in Figure 7 as individual vectors for each angle of attack. The theoretical Sears function (corrected to reflect the actual lift curve slope for the tested airfoil) is also shown with the additional corrections resulting from horizontal flow fluctuations for several reduced frequencies.

RESULTS

The experimental values of the Sears function (unsteady lift) at various angles of attack are shown in Figure 7, as vectors in the phase-plane. They have been converted by the factor exp(-ik) to a phase relative to the passage of the sinusoidal gust at the leading edge of the airfoil, as utilized in Reference 14. In the higher range of reduced frequency, the theoretical lift lags the interaction of the gust with the leading edge by an eighth of an oscillation period, as mentioned previously, so the theoretical vectors lie on the -45 degree line with an amplitude of $1/\sqrt{2\pi k}$. This amplitude is based on a lift-curve slope of 2π, substantially higher than that shown in Figure 6 for the actual airfoil. Accordingly, the theoretical magnitude for a reduced frequency of 3.9 is shown in Figure 7, corrected by the ratio of actual to idealized lift curve slopes. This is felt to be an improved basis for comparison with experimental values, in accordance with successful modifications of a similar nature made in Reference 15 for sectional unsteady response coefficients of finite-span wings.

Figure 7 shows that the experimental response is perhaps 50 percent larger than the adjusted Sears function at low angles of attack, falling off slightly at higher angles substantially past static stall. The phase relationship is close to that predicted theoretically, although a gradual increase of lag is noted at the higher angles.

Sears (Reference 11) established the unsteady lift and moment on an airfoil in a transverse sinusoidally varying flow field without the necessity of establishing the unsteady pressure distribution. His result, that the unsteady lift always acts at the quarter chord location, implies that there is no pressure wave phenomenon present which would cause the center of pressure to fluctuate with time. This result tends to defy intuition in the sense that one would certainly expect the instantaneous pressure at different chordwise locations to respond differently to the varying vertical velocities across the chord. To check this intuitive logic, the raw output from several pressure transducers was displayed on an oscilloscope and photographed. The results are presented in Figure 8. Picture (a) clearly shows a phase shift between the 10 and 90 percent chord stations on the suction side of the airfoil with the trailing edge leading the leading edge. Picture (b) shows the expected out-of-phase response of the 10 percent chord transducers on opposite sides of the airfoil. In picture (c), no apparent phasing can be noted between 10 and 90 percent chord stations on the pressure surface of the airfoil. To make certain that (c) did not represent a 360 deg phase shift, two intermediate chordwise stations were included with the results shown in picture (d). All transducers on the pressure surface were roughly in phase while on the suction surface, trailing edge pressures led leading edge pressures.

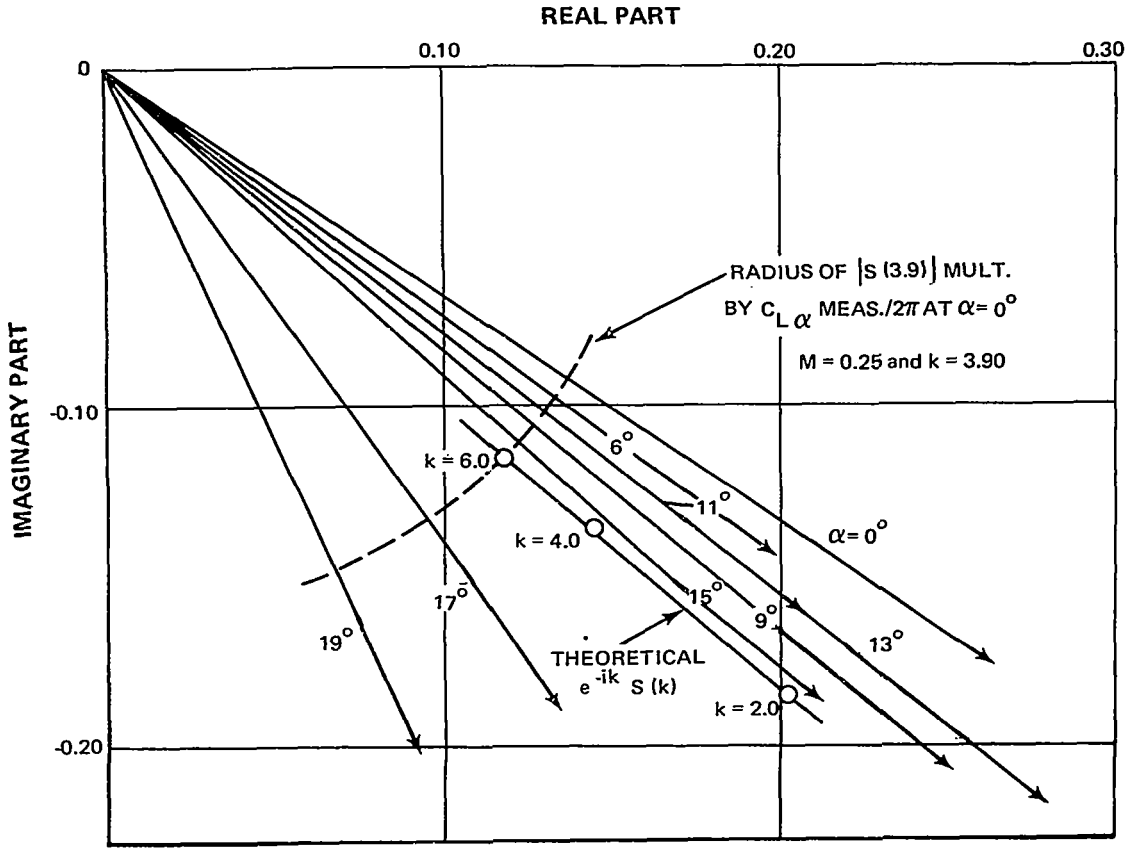

Figure 7 Experimental Values of Sears Function at Various Angles of Attack Multiplied by e^{-ik}

The effect of the measured airfoil response on predicted broadband noise is slight, since it is only an increase corresponding to the 50 percent greater response. While this is very significant for buffeting or flutter, the logarithmic response of the ear equates it to a mere 3.5 db rise in predicted noise level. However, either with or without this correction, the predicted level is significant.

Figure 5 shows the predicted noise spectrum to 6 khz, within the inlet of a configuration from a recent design study and based on a 1 lb per ft. fluctuating load on the fan blades. The spectrum of this fluctuation is assumed to be constant to 5 khz, then drops off exponentially. The assumed configuration is a fan of 46 blades operating at 2300 rpm in an annular duct of 0.576 hub-tip ratio with an outer radius of 3.87 ft. Axial Mach number of the flow is 0.296 and the blade angle is uniform at 40 degrees. The field point is 2.0 feet ahead of the compressor at a radius of 3.8 ft.

The 110 db level of the power spectral density is consistent with experimental observations, and indicative of the potential importance of turbulence/blade interaction as a source of broadband noise. The 1 lb per foot load fluctuation is compatible with that expected on the blades due to inlet turbulence of 0.1 to 1.0 percent, such as might occur from wakes of upstream struts, acoustically-treated splitters, etc.

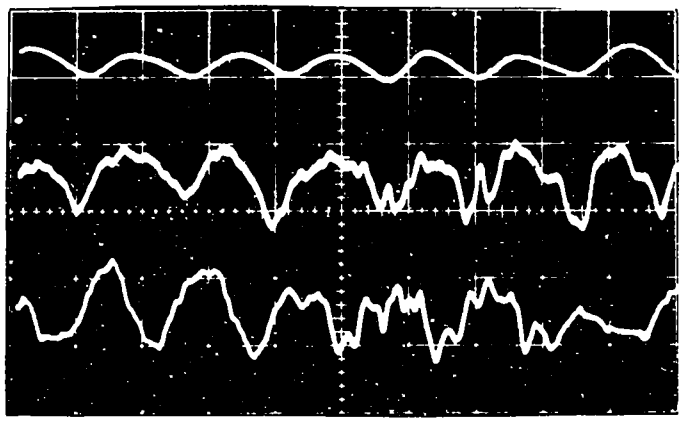

(a) PITRAN, 10% CHORD AND 90% CHORD PRESSURES - SUCTION SIDE OF AIRFOIL

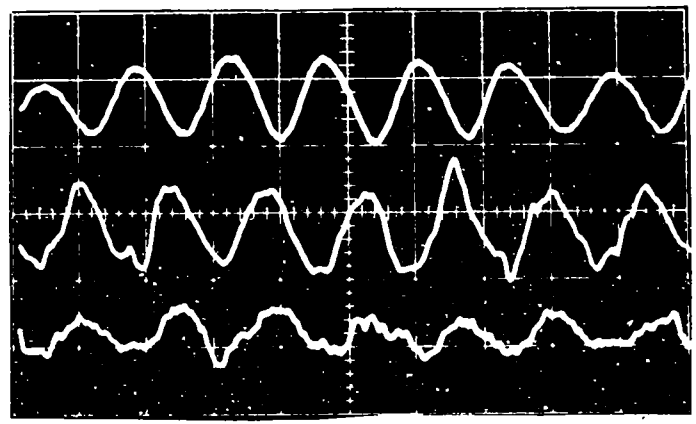

(c) PITRAN, 10% CHORD AND 90% CHORD PRESSURES - PRESSURE SIDE OF AIRFOIL

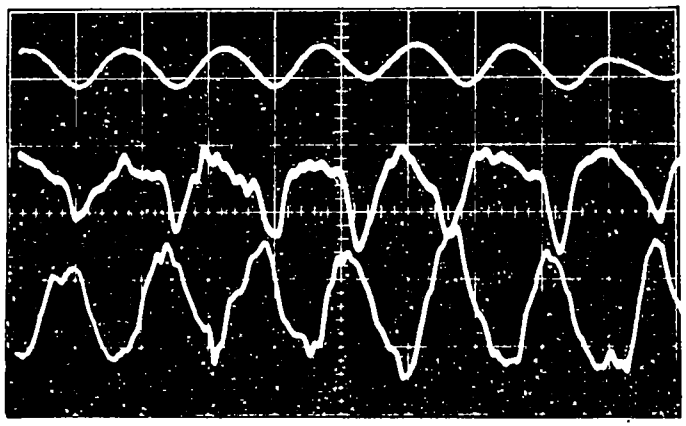

(b) PITRAN, 10% CHORD ON SUCTION SIDE, 10% CHORD ON PRESSURE SIDE

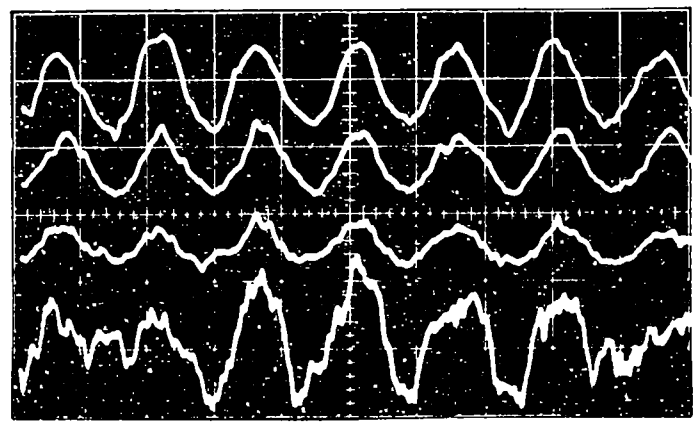

(d) 10%, 30%, 60% & 90% CHORD PRESSURES ON PRESSURE SIDE OF AIRFOIL

Figure 8 Oscilloscope Pictures of Time Varying Pressure Signals

VI REFERENCES

1. Tyler, J. M., and Sofrin, T. G., "Axial Flow Compressor Noise Studies," SAE Trans., 1961, Vol. 70, pp. 309-332.

2. Morfey, C. L., "Rotating Pressure Patterns in Ducts: Their Generation and Transmission," J. Sound and Vibr., 1964, Vol. 1, pp. 60-87.

3. Ribner, H. S., "Convection of a Pattern of Vorticity Through a Shock Wave," NACA Report 1164, 1954.

4. Ribner, H. S., "Shock-Turbulence Interaction and the Generation of Noise, " NACA Report 1233, 1955.

5. Lowson, M. V., "Pressure Fluctuations Resulting From Shock Interaction," J. Sound and Vibr., 1968, Vol. 7, pp. 380-392.

6. Kemp, N. H., and Sears, W. R., "Aerodynamic Interference Between Moving Blade Rows," J. Aero. Sci., 1953, Vol. 20, pp. 585-598.

7. Kerrebrock, J. L., "The Interaction of Flow Discontinuities with Small Disturbances in a Compressible Fluid." Ph. D. Thesis, Cal. Inst. of Tech., 1956.

8. Moore, F. K., "Unsteady Oblique Interaction of a Shock Wave with a Plane Disturbance." NACA Report 1165, 1954.

9. Ribner, H. S., "Acoustic Energy Flux from Shock-Turbulence Interaction." J. Fluid Mech. Vol. 35, (2), 1969 pp. 299-310.

10. Batchelor, G. K., "The Theory of Homogeneous Turbulence." Cambridge Univ. Press, 1953.

11. Sears, William R., "Some Aspects of Non-Stationary Airfoil Theory and Its Practical Application." Jour. Aero. Sci., Vol. 8, pp. 104-108, January 1941.

12. Horlock, J. H., "Fluctuating Lift Forces on Airfoils Moving Through Transverse and Chordwise Gusts." A.S.M.E. Paper No. 68-FE-28, 1968.

13. Ruger, C., and S. Slutsky, "Broadband Noise Field of a Rotor Using the Method of Green's Functions," General Applied Science Laboratory, TR-712, 1968. Prepared for Pratt & Whitney Aircraft under private contract.

14. Arnoldi, R. A., "Unsteady Airfoil Response," pp. 247-256 in NASA SP-207, "Basic Aerodynamic Noise Research," 1969.

15. Yates, E. C., Jr., "Modified-Strip-Analysis Method for Predicting Wing Flutter at Subsonic to Hypersonic Speeds," J. Aircraft, Vol. 3, pp. 25-29, 1966.

APPENDIX A

SUMMARY OF KERREBROCK'S ANALYSIS (REFERENCE 7)

The analysis of Kerrebrock (Reference 7) has been used as a basis for this work. Since it is an unpublished Ph.D. thesis and not readily available, a brief summary of it appears here.

Elementary disturbances upstream of a shock wave are related to disturbances downstream of a shock wave by using a perturbation technique with the one-dimensional shock relations. The resulting equations are:

$$\frac{u_1'}{U_1'} = b_1 \frac{u_1}{U_1} + b_2 \frac{s}{c_p} + b_3 \frac{p}{P} \tag{A-1}$$

$$\frac{p'}{P'} = b_4 \frac{u_1}{U_1} + b_5 \frac{s}{c_p} + b_6 \frac{p}{P} \tag{A-2}$$

$$\frac{s'}{c_p} = b_7 \frac{u_1}{U_1} + b_8 \frac{s}{c_p} + b_9 \frac{p}{P} \tag{A-3}$$

where

$$b_1 = 1 - 2\,b_2$$

$$b_2 = 1 - \frac{\gamma - 1}{\gamma + 1} m$$

$$b_3 = \frac{\gamma - 1}{\gamma}\, b_2$$

$$b_4 = \frac{4\gamma}{\gamma + 1}\, m\, M_1'^2$$

$$b_5 = \frac{b_4}{2}$$

$$b_6 = 1 - \frac{\gamma - 1}{2\gamma} b_4$$

$$b_7 = \frac{b_4}{\gamma} - 2\,b_2$$

$$b_8 = 1 + b_2 + \frac{b_4}{2\gamma}$$

$$b_9 = \frac{\gamma - 1}{\gamma} b_2 - \frac{\gamma - 1}{2\gamma^2}\, b_4 \tag{A-4}$$

The small fluctuating quantities, which will be represented by stochastic Fourier integrals, obey the following differential equations, which are derived from the inviscid equations of motion by using a perturbation technique. The equations (to first order) are:

$$\left(\frac{\partial}{\partial t} + U \frac{\partial}{\partial X_1}\right) \underline{u} + \frac{1}{\rho} \nabla p = 0 \tag{A-5}$$

$$\left(\frac{\partial}{\partial t} + U \frac{\partial}{\partial X_1}\right) p = a^2 \nabla^2 p \tag{A-6}$$

$$\left(\frac{\partial}{\partial t} + U \frac{\partial}{\partial X_1}\right) s = 0 \tag{A-7}$$

It can be shown that the vorticity disturbance ($\underline{\Omega} = \nabla \times \underline{u}$) is independent of the other disturbances by taking the curl of equation (A-5). Thus the velocity field is split into two parts; one compressible, irrotational associated with the pressure field, and the other incompressible, rotational associated with the vorticity field.

$$\underline{u} = \underline{u}_p + \underline{u}_v$$

where

$$\nabla \cdot \underline{u}_v = 0$$

$$\nabla \times \underline{u}_p = 0$$

The coordinate system is transformed and the disturbances are expressed by stochastic Fourier integrals.

$$\frac{\underline{u}_v}{U_1} = \int e^{i [k_{1v} (\xi - U_1 t) + k_{2v} \eta + k_{3v} X_3]} \frac{d\underline{Z}_v (\underline{k}_v)}{\sin(\sigma)} \tag{A-8}$$

$$\frac{s}{c_p} = \int e^{i [k_{1s} (\xi - U_1 t) + k_{2s} \eta + k_{3s} X_3]} dZ_s(\underline{k}_s) \tag{A-9}$$

$$\frac{p}{P} = \int e^{i[k_{1p} (\xi - U_1 t) + k_{2p} \eta + k_{3p} X_3) - a k_p t]} dZ_p (\underline{k}_p) \tag{A-10}$$

$$\frac{\underline{u}_p}{U_1} = \int \frac{1}{\gamma M_1} e^{i [k_{1p} (\xi - U_1 t) + k_{2p} \eta + k_{3p} X_3 - a k_p t]} \frac{\underline{k}_p}{k_p} dZ_p(\underline{k}_p) \tag{A-11}$$

ξ is a coordinate axis normal to the plane of the shock (the $\eta - X_3$ plane). The various coordinate systems used appear below in Figure A-1.

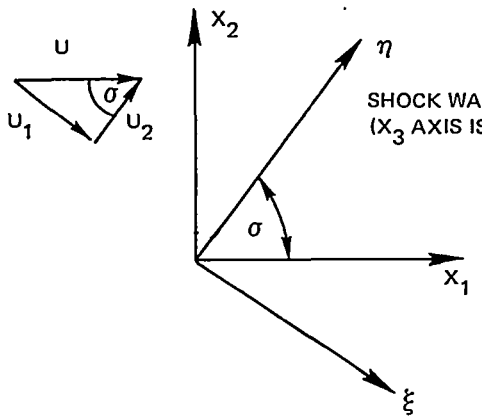

Figure A-1

Coordinate Systems

Equations similar to A-8 through A-11 apply downsteam of the shock wave also and the elementry Fourier components are assumed to satisfy the differential equations shown above. The wave numbers of disturbances downstream of the shock wave are found in terms of the wave numbers of disturbances upstream of the shock by matching periodicity (frequency) at the shock wave. These relationships depend on whether or not the upstream disturbance is a propagating or non-propagating disturbance. For non-propagating upstream disturbances:

$$k_1 U_1 = k_1' U_1' = k_{1p}' U_1' + k_p' a' \qquad \text{(primes indicate downstream of shock wave)}$$

$$k_4 = \sqrt{k_2^2 + k_3^2} = k_4' = k_{4p}' \qquad \text{(A-12)}$$

For propagating upstream disturbances:

$$k_{1p} U_1' + k_p a = k_1' U_1' = k_{1p}' U_1' + k_p' a'$$

$$k_{4p} = k_4' = k_{4p}' \qquad \text{(A-13)}$$

It is convenient to express the wave numbers in spherical polar coordinates defined below and shown in Figure A-2.

Figure A-2

Spherical Polar Representation
of Wave Numbers

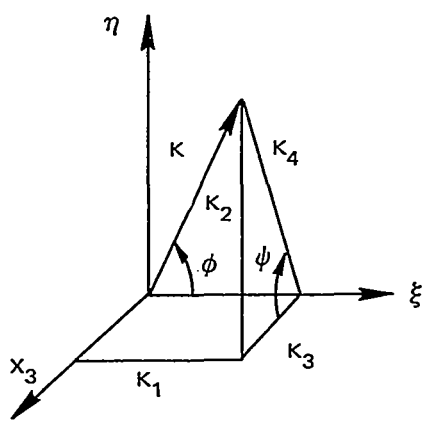

From Figure A-2, it is easily seen that the coordinate transformation is

$$k_1 = k \cos(\phi) \qquad o \leqslant k \leqslant \infty$$

$$k_2 = k \sin(\phi) \sin(\psi) \qquad o \leqslant \phi \leqslant \pi$$

$$k_3 = k \sin(\phi) \cos(\psi) \qquad o \leqslant \psi \leqslant 2\pi \qquad \text{(A-14)}$$

It is assumed that the passage of a wavefront causes the shock wave to be deflected locally from the plane of the shock by a small angle and that this disturbance travels along the shock plane with a speed which depends on the type of disturbance and the inclination of the wave fronts. When this is taken into account and one assumes that the integrands of equations A-8 through A-11 obey equations A-1 through A-3, one obtains the following results after lengthy manipulations:

$$\frac{dZ_{1v}'}{\sin(\sigma)} = S_{1v}^{1v} \frac{dZ_{1v}}{\sin(\sigma)} + S_{1v}^{p} dZ_p + S_{1v}^{s} dZ_s \qquad \text{(A-15)}$$

$$dZ_p' = S_p^{1v} \frac{dZ_{1v}}{\sin(\sigma)} + S_p^{p} dZ_p + S_p^{s} dZ_s \qquad \text{(A-16)}$$

$$dZ_s' = S_s^{1v} \frac{dZ_{1v}}{\sin(\sigma)} + S_s^{p} dZ_p + S_s^{s} dZ_s \qquad \text{(A-17)}$$

where

$$\Delta_v S_{1v}^{1v} = b_1 - \frac{a_3}{\tan^2(\phi_v)} - \frac{a_2 M_1'^2}{1 - M_1' X_v}\left[m^2 a_1 - (m - 1 + \frac{m}{\tan^2(\phi_v)})(1 - \frac{X_v}{M_1'})\right] \qquad \text{(A-18)}$$

$$\Delta_p S_{1v}^{p} = b_3 + \frac{\sin(\phi_p)}{\gamma M_1}\left[\frac{b_1}{\tan(\phi_p)} + \frac{a_3}{y}\right] - \frac{m a_1}{\gamma(1 - M_1' Z)}\left[\frac{a_3}{m} - \frac{(\gamma-1)}{2\gamma} b_4 + \frac{m}{m-1}\frac{b_4}{\gamma M_1}\cos(\phi_p)\right.$$

$$\left. - (b_6 - \frac{b_4}{\gamma M_1}(\frac{m}{(m-1)y} - \frac{1}{\tan(\phi_p)})\sin(\phi_p))\frac{(1 - \frac{Z}{M_1'})}{m a_1}\right] \qquad \text{(A-19)}$$

$$\Delta_s S^s_{1v} = b_2 + \frac{2m}{\gamma+1} \frac{M_1'^2}{1 - M_1' X_s} \left[m a_1 - 1 + \frac{X_s}{M_1'} \right] \quad \text{(A-20)}$$

$$\Delta_v S^{1v}_p = b_4 \left(1 - \frac{m}{\tan^2(\phi_v)}\right) \quad \text{(A-21)}$$

$$\Delta_p S^p_p = \frac{-mb_4}{m-1} \left[\frac{\sin(\phi_p)}{\gamma y M_1} + \frac{1}{y^2} \left(b_3 + \frac{b_1 \cos(\phi_p)}{\gamma M_1}\right) \right] + \left(1 - \frac{a_3}{y^2}\right) \left[b_6 + \frac{b_4 \cos(\phi_p)}{\gamma M_1} \right] \quad \text{(A-22)}$$

$$\Delta_s S^s_p = \frac{-b_4}{2} \left(1 - \frac{m}{\tan^2(\phi_s)}\right) \quad \text{(A-23)}$$

$$\Delta_v S^{1v}_s = b_7 \left(1 - \frac{m}{\tan^2(\phi_v)}\right) \quad \text{(A-24)}$$

$$S^p_s = b_9 + \frac{b_7}{m-1} \left(\frac{\sin(\phi_p)}{\gamma M_1} \left(\frac{m-1}{\tan(\phi_p)} - \frac{m}{y} \right) - \frac{m}{y^2} S^p_{1v} + \frac{m a_1}{\gamma} \left(\frac{S^p_p}{1 - M_1' Z} \right) \right) \quad \text{(A-25)}$$

$$\Delta_s S^s_s = b_8 - \frac{m}{\tan^2(\phi_s)} \left(b_8 + \frac{2b_2}{m-1} \right) - \frac{m a_1 a_2 M_1'^2}{(1 - M_1' X_s)} \left(1 - \frac{\left(1 - \frac{X_s}{M_1'}\right)}{a_1 \tan^2(\phi_s)} \right) \quad \text{(A-26)}$$

$$\Delta_v = 1 - \frac{a_3}{\tan^2(\phi_v)} - \frac{m a_1 a_2 M_1'^2}{(1 - M_1' X_v)} \left(1 - \frac{\left(1 - \frac{X_v}{M_1'}\right)}{a_1 \tan^2(\phi_v)} \right) \quad \text{(A-27)}$$

$$\Delta_s = 1 - \frac{a_3}{\tan^2(\phi_v)} - \frac{m a_1 a_2 M_1'^2}{(1 - M_1' X_s)} \left(1 - \frac{\left(1 - \frac{X_s}{M_1'}\right)}{a_1 \tan^2(\phi_s)} \right) \quad \text{(A-28)}$$

$$\Delta_p = 1 - \frac{a_3}{y^2} - \frac{m\, a_1\, a_2\, M_1'^2}{(1 - M_1'\, Z)} \left(1 - \frac{\left(1 - \frac{Z}{M_1'}\right)}{a_1\, y^2} \right) \qquad \text{(A-29)}$$

$$a_1 = \frac{1 - M_1'^2}{m^2\, M_1'^2}$$

$$a_2 = \frac{4\, m}{(\gamma+1)\,(m-1)}$$

$$a_3 = \frac{m}{m-1} \left(1 + \frac{3-\gamma}{\gamma+1}\, m \right)$$

$$X_{v,s} = \sqrt{1 - a_1 \tan^2(\phi_{v,s})}$$

$$Z = \sqrt{1 - a_1\, y^2}$$

$$y = \frac{\sin(\phi_p)}{\cos(\phi_p) + \frac{1}{M_1}} \qquad \text{(A-30)}$$

The spectral function of the pressure disturbance downstream of a shock wave can be found in terms of the spectral functions of the disturbances upstream of the shock wave. Batchelor (Reference 10) shows how the spectral function of a homogeneous disturbance is related to the Fourier coefficients of the disturbance field in the following way,

$$\Phi_{ii}\,(\underline{k}_i)\;\; d\,\underline{k}_i = \overline{d\,Z_i^{\bullet}\,(\underline{k}_i)\;\; d\,Z_i\,(\underline{k}_i)} \qquad \text{(A-31)}$$

Using this and equation A-16, which relates the Fourier coefficients of the downstream pressure waves to the Fourier coefficients of the upstream disturbances, one can obtain the spectral function of the downstream pressure disturbance in terms of the spectral functions of the upstream disturbances:

$$\Phi'_{pp}\ (\underline{k}'_p)\ d\underline{k}'_p = \left| S_p^{1v} \right|^2 \frac{\overline{d Z^*_{1v}}}{\sin(\sigma)} \frac{d Z_{iv}}{\sin(\sigma)} + \left| S_p^s \right|^2 \overline{d Z_s^*\ d Z_s} + \left| S_p^p \right|^2 \overline{d Z_p^*\ d Z_p}$$

or

$$\Phi'_{pp}\ (\underline{k}'_p)\ d\underline{k}'_p = \left| S_p^{1v} \right|^2 \Phi_{vv}\ (\underline{k}_v)\ d\underline{k}_v + \left| S_p^s \right|^2 \Phi_{ss}\ (\underline{k}_s)\ d\underline{k}_s + \left| S_p^p \right|^2 \Phi_{pp}\ (\underline{k}_p)\ d\underline{k}_p$$

The wave number vectors upstream of the shock wave are related to the wave number vector downstream of the shock wave (ie., equations A-12 and A-13. Thus by using the Jacobians of these transformations the following is obtained,

$$\Phi'_{pp}\ (\underline{k}'_p) = 2\left(\left| S_p^{1v} \right|^2 \Phi_{vv}(\underline{k}_v)\, J\left(\frac{\underline{k}_v}{\underline{k}'_p}\right) + \left| S_p^s \right|^2 \Phi_{ss}\ (\underline{k}_s)\, J\left(\frac{\underline{k}_s}{\underline{k}'_p}\right)\right) + \left| S_p^p \right|^2 \Phi_{pp}(\underline{k}_p)\, J\left(\frac{\underline{k}_p}{\underline{k}'_p}\right)$$

(the factor of 2 arises because as k_{1v} and k_{1s} vary from $-\infty$ to $+\infty$, k'_{1p} varies over this range twice). It is convenient to express this in the spherical polar coordinates defined by equation A-14, thus

$$\Phi'_{pp}\ (k'_p, \phi'_p, \psi'_p) = \Phi'_{pp}\ (k'_p)\ J\left(\frac{\underline{k}'_p}{k'_p, \phi'_p, \psi'_p}\right) \qquad \text{(A-32)}$$

Consider the case where the upstream disturbance consists of a vorticity type disturbance only; then

$$\Phi'_{pp}\ (k'_p, \phi'_p, \psi'_p) = 2\left| S_p^{1v} \right|^2 \Phi_{vv}\ J\left(\frac{\underline{k}_v}{\underline{k}'_p}\right) J\left(\frac{\underline{k}'_p}{k'_p, \phi'_p, \psi'_p}\right) \qquad \text{(A-33)}$$

For isotropic homogeneous turbulence Batchelor shows that the spectral function of the component of the velocity disturbance normal to the shock is

$$\Phi_{vv} = \frac{E(k_v)}{4\pi k_v^2} \left(1 - \left(\frac{k_{1v}}{k_v}\right)^2\right) \tag{A-34}$$

where $E(k_v)$ is the energy-spectrum function having the property

$$\int_0^\infty E(k_v)\, dkv = \frac{3}{2} \overline{u_{1v}^2} \tag{A-35}$$

Substituting the spectral functions of the turbulence A-34 into the equation for the spectral function of the pressure disturbance downstream of the shock the following is obtained after evaluating the Jacobians

$$\Phi'_{pp}(k'_p, \phi'_p, \psi'_p) = \left|S_p^{1v}\right|^2 \frac{E(k_v)\sin^2\phi_v}{2\pi k_v^2 U_1^2} \frac{1}{m}\left(1 + \frac{\cos\phi'_p}{m'_1}\right)k_p'^2 \sin\phi'_p$$

It is convenient to express Φ'_{pp} in terms of k_v since one can then relate the pressure spectral function to the intensity of the turbulence using equation A-35. The spectral function for the pressure disturbance downstream of a shock wave due to turbulence upstream of the shock wave becomes:

$$\Phi'_{pp}(k_v, \phi'_p, \psi'_p) = \frac{\frac{1}{m}\left(1 + \frac{\cos\phi'_p}{M'_1}\right)\sin^3\phi'_p}{\left(\left(\frac{1}{m}(\cos\phi'_p + \frac{1}{M'_1})\right)^2 + \sin^2\phi'_p\right)^{5/2}} \frac{E(k_v)}{2\pi U_1^2} \left|S_p^{1v}\right|^2 \tag{A-36}$$

APPENDIX B

SUMMARY OF BROADBAND NOISE ANALYSIS OF REFERENCE 13

A Pratt & Whitney Aircraft analysis of the generation and propagation of broadband noise due to randomly fluctuating lift on rotor blades in a compressor has been programmed for use on the Univac 1108 digital computer. The analysis computes the broadband noise produced in an annular duct by arbitrary (but specified) randomly fluctuating lift on rotor blades. Thus, it provides an essential element in the complex analysis of broadband noise from compressors. A detailed mathematical formulation was provided by the General Applied Science Laboratory in Reference 13 under private contract to Pratt & Whitney Aircraft.

The theory of broadband noise developed in Reference 13 is based on the following expansion obtained from the Green's function, relating the acoustic pressure at a single frequency (Fourier transform of pressure) to the corresponding stress distribution components σ_x and σ_θ.

Above Cutoff:

$$p'_\omega(\bar{x}) = \frac{1}{4\pi} \sum_{m=-\infty}^{\infty} \sum_{\mu=1}^{\infty} R_{m\mu}(r)\, e^{im\theta} \int_0^{2\pi} \int_h^1 \left[\frac{r_o \sigma_x}{1-M^2} \left(\operatorname{sgn} x \right.\right.$$

$$\left.\left. - \frac{|\omega| M}{\sqrt{\omega^2 - \kappa_{m\mu}^2 (1-M^2)}} \right) + \frac{m \operatorname{sgn} \omega \sigma_\theta}{\sqrt{\omega^2 - \kappa_{m\mu}^2 (1-M^2)}} \right] R_{m\mu}(r_o)\, e^{-im\theta_o}$$

$$\cdot \exp\left[\frac{i |x| \operatorname{sgn} \omega}{1-M^2} \sqrt{\omega^2 - \kappa_{m\mu}^2 (1-M^2)} \right] \exp\left[-\frac{i\omega M x}{1-M^2} \right] dr_o\, d\theta_o \qquad \text{(B-1)}$$

Below Cutoff:

$$p'_\omega(\bar{x}) = \frac{1}{4\pi} \sum_{m=-\infty}^{\infty} \sum_{\mu=1}^{\infty} R_{m\mu}(r)\, e^{im\theta} \int_0^{2\pi} \int_h^1 \left[\frac{r_o \sigma_x}{1-M^2} \left(\operatorname{sgn} x \right.\right.$$

$$\left.\left. + \frac{i\omega M}{\sqrt{\kappa_{m\mu}^2 (1-M^2) - \omega^2}} \right) - \frac{im\sigma_\theta}{\sqrt{\kappa_{m\mu}^2 (1-M^2) - \omega^2}} \right] R_{m\mu}(r_o)\, e^{-im\theta_o}$$

$$\exp\left[-\frac{|x|}{1-M^2}\sqrt{\kappa_{m\mu}^2\ (1-M^2)-\omega^2}\right]\ \exp\left[-\frac{i\omega Mx}{1-M^2}\right]dr_o\ d\theta_o \qquad \text{(B-2)}$$

where

$$\text{sgn}\ \alpha = \begin{cases} 1 \text{ for } \alpha > 0 \\ -1 \text{ for } \alpha > 0 \end{cases}$$

If the stress fluctuations are assumed coherent over the span of the blade, the spanwise dependence of fluctuation amplitudes may be expressed in terms of modal coefficients $\bar{f}_{m\mu}$ representing the contribution of each acoustic mode $R_{m\mu}$ (r) to the representation of the spanwise dependence. In the tangential direction, the fluctuations on adjacent blades are assumed to be completely uncorrelated. The time-dependent factor in the stress fluctuation, g(t), is formed into a power spectral function $G(\omega)$ as in equation 14. In terms of this function, and hence in terms of the turbulence spectrum $V(\omega)$ as in equation 16, the acoustic power spectral function then becomes:

Above Cutoff

$$P_x(\bar{x}',\omega) = \frac{B\sin^2\epsilon}{8\pi^2\ \rho_o^2\ c^4\ R_o^2\ (1-M^2)^2}\ \sum_{\mu=1}^{\infty}\sum_{\mu'=1}^{\infty}\sum_{m} C_{\mu\mu'}$$

$$\cdot\ \bar{f}^x_{m\mu}\ \bar{f}^x_{m\mu'}\ R_{m\mu}(r)\ R_{m\mu'}(r)\ G(\omega+m\Omega)\left[\text{sgn}\ x - \frac{|\omega|\ M}{\sqrt{\omega^2-\kappa_{m\mu}^2\ (1-M^2)}}\right]\left[\text{sgn}\ x - \frac{|\omega|\ M}{\sqrt{\omega^2-\kappa_{m\mu'}^2\ (1-M^2)}}\right]$$

$$\cdot\ \cos\left[\frac{|x|\ \text{sgn}\ \omega}{1-M^2}\left(\sqrt{\omega^2-\kappa_{m\mu}^2\ (1-M^2)}-\sqrt{\omega^2-\kappa_{m\mu'}^2\ (1-M^2)}\right)\right] \qquad \text{(B-3)}$$

where $$C_{\mu\mu'} = \begin{cases} 1 & \mu \neq \mu' \\ \tfrac{1}{2} & \mu = \mu' \end{cases}$$

$$P_{x,\theta}\ (\bar{x},\omega) = \frac{B\ \sin\ \epsilon\ \cos\ \epsilon}{8\pi^2\ \rho_o^2\ c^4\ R_o^2\ (1-M^2)} \sum_{\mu,\mu'} \sum_{m} m\ \bar{f}^{x}_{m\mu} \cdot \bar{f}^{\theta}_{m\mu'}$$

$$\cdot\ R_{m\mu}\ (r)\ R_{m\mu'}\ (r)\ G\ (\omega+m\Omega) \left[\text{sgn}\ x - \frac{|\omega|\ M}{\sqrt{\omega^2 - \kappa^2_{m\mu}\ (1-M^2)}} \right]$$

$$\cdot \left[\frac{\text{sgn}\ (\omega)}{\sqrt{\omega^2 - \kappa^2_{m\mu'}\ (1-M^2)}} \right] \cos\left[\frac{|\dot{x}|\ \text{sgn}\ (\omega)}{1-M^2} \left(\sqrt{\omega^2 - \kappa^2_{m\mu}\ (1-M^2)} \right.\right.$$

$$\left.\left. - \sqrt{\omega^2 - \kappa^2_{m\mu'}\ (1-M^2)} \right) \right] \qquad \text{(B-4)}$$

$$P_{\theta}\ (\bar{x},\omega) = \frac{B\ \cos^2\ \epsilon}{8\pi^2\ \rho_o^2\ c^4\ R_o^2} \sum_{\mu=1}^{\infty} \sum_{\mu'=1}^{\mu} \sum_{m} m^2\ C_{\mu\mu'}\ R_{m\mu}(r)$$

$$\cdot\ \bar{f}^{\theta}_{m\mu}\ \bar{f}^{\theta}_{m\mu'}\ R_{m\mu'}\ (r)\ G\ (\omega + m\Omega) \left(\frac{1}{\sqrt{\omega^2 - \kappa^2_{m\mu}\ (1-M^2)}} \right)$$

$$\cdot \left(\frac{1}{\sqrt{\omega^2 - \kappa^2_{m\mu'}\ (1-M^2)}} \right) \cos \left[\frac{|\dot{x}|\ \text{sgn}\ \omega}{1-M^2} \left(\sqrt{\omega^2 - \kappa^2_{m\mu}\ (1-M^2)} \right.\right.$$

$$\left.\left. - \sqrt{\omega^2 - \kappa^2_{m\mu'}\ (1-M^2)} \right) \right] \qquad \text{(B-5)}$$

Below Cutoff:

$$P_x(x,\omega) = \frac{B \sin^2 \epsilon}{16\pi^2 \rho_o^2 c^4 R_o^2 (1-M^2)^2} \sum_{\mu,\mu'} \sum_{m} \bar{f}^x_{m\mu} \bar{f}^{-x}_{m\mu'}$$

$$\cdot R_{m\mu}(r) R_{m\mu'}(r) G(\omega+m\Omega) \left[(\text{sgn } x)^2 + \frac{(\omega M)^2}{\sqrt{\kappa^2_{m\mu}(1-M^2)-\omega^2}\ \sqrt{\kappa^2_{m\mu'}(1-M^2)^2}} \right] \exp\left[-\frac{|x|}{1-M^2} \left[\sqrt{\kappa^2_{m\mu}(1-M^2)-\omega^2} + \sqrt{\kappa^2_{m\mu'}(1-M^2)-\omega^2} \right] \right] \quad \text{(B-6)}$$

$$P_{x,\theta}(\bar{x},\omega) = -\frac{B \sin \epsilon \cos \epsilon}{8\pi^2 \rho_o^2 c^4 R_o^2 (1-M^2)} \sum_{\mu,\mu'} \sum_{m} m \bar{f}^x_{m\mu} \bar{f}^{\theta}_{m\mu'}$$

$$\cdot R_{m\mu}(r) R_{m\mu'}(r) G(\omega+m\Omega) \left[\frac{\omega M}{\sqrt{\kappa^2_{m\mu}(1-M^2)-\omega^2}} \right] \left[\frac{1}{\sqrt{\kappa^2_{m\mu'}(1-M^2)-\omega^2}} \right]$$

$$\exp\left[-\frac{|x|}{1-M^2} \left(\sqrt{\kappa^2_{m\mu}(1-M^2)-\omega^2} + \sqrt{\kappa^2_{m\mu'}(1-M^2)-\omega^2} \right) \right] \quad \text{(B-7)}$$

$$P_\theta(\bar{x},\omega) = \frac{B \cos^2 \epsilon}{16\pi^2 \rho_o^2 c^4 R_o^2} \sum_{\mu,\mu'} \sum_{m} m^2 \bar{f}^{\theta}_{m\mu'} \bar{f}^{\theta}_{m\mu}$$

$$\cdot R_{m\mu}(r) R_{m\mu'}(r) G(\omega+m\Omega) \left[\frac{1}{\sqrt{\kappa^2_{m\mu}(1-M^2)-\omega^2}} \right] \left[\frac{1}{\sqrt{\kappa^2_{m\mu'}(1-M^2)-\omega^2}} \right]$$

$$\exp\left\{ - \frac{|x|}{1-M^2} \left[\sqrt{\kappa^2_{m\mu} (1-M^2) - \omega^2} + \sqrt{\kappa^2_{m\mu'} (1-M^2) - \omega^2} \right] \right\} \qquad \text{(B-8)}$$

APPENDIX C

COMBINED RESPONSE TO VERTICAL AND HORIZONTAL FLUCTUATIONS

Application of the continuity equation to velocity fluctuations superposed on a horizontal steady flow shows that the horizontal velocity fluctuation leads the vertical velocity fluctuation by 90 degrees, which was also consistently measured in the experiment. However, the theory also predicts equal amplitudes for the two fluctuations, whereas in practice the horizontal fluctuation was approximately one-third the amplitude of the vertical fluctuation. Thus, in the analysis which follows, it will be more convenient to treat these fluctuations as separate entities, $ve^{i\omega t}$ for the vertical fluctuation and $iue^{i\omega t}$ for the horizontal.

From Sears (Reference 11) and from Horlock (Reference 12) the total fluctuating lift amplitude due to combined vertical and horizontal velocity fluctuations is:

$$2\pi \rho U b e^{i\omega t} \left[v\,S(k) + iu\alpha\,T(k) \right] \tag{C-1}$$

Non-dimensionalizing to obtain a fluctuating lift coefficient and separating the real and imaginary parts,

$$C_L = C_{L_R} + iC_{L_I} = \frac{2\pi v}{U}\left[S_R + iS_I + \frac{u\alpha}{v}\left(iT_R - T_I \right) \right] \tag{C-2}$$

An adjustment has been made to these theoretical formulas to reflect the difference between the theoretical lift curve slope, 2π, and the experimental value of 5.14 obtained from Figure 6. This value and the measured ratio of $u/v = 0.368$ were used to calculate the results described in the main body of this report. Departure of the u/v ratio from the value of unity derived for an irrotational flow indicates the presence of vorticity, presumably due to turbulent diffusion from the centers of circulation on the Karman vortex wake of the cylinder.